J Neurooncol (2016) 127:243–251
DOI 10.1007/s11060-015-2041-5

LABORATORY INVESTIGATION

Multiparametric MR imaging of tumor response to intraarterial chemotherapy in orthotopic xenograft models of human metastatic brain tumor

Byungjun Kim[1] · Keonha Kim[2] · Keun Ho Im[2] · Jae-Hoon Kim[2] · Jung Hee Lee[2] · Pyoung Jeon[2] · Hongsik Byun[2]

Received: 22 September 2015 / Accepted: 28 December 2015 / Published online: 8 January 2016

Abstract The purpose of our study was to investigate the therapeutic efficacy of intraarterial (IA) chemotherapy via multiparametric magnetic resonance imaging (MRI) analysis in orthotopic mouse brain tumor models. Stereotactic-guided intracranial inoculation of MDA-MB-231 cells was performed in nude mice. Thirty tumor bearing mice were randomized into three groups, and each group received either IA docetaxel administration ($n = 10$), intravenous (IV) docetaxel administration ($n = 10$), or IA solvent injection ($n = 10$) as control. Treatment response was monitored by diffusion-weighted imaging and dynamic contrast enhanced-MRI obtained 1 day before and 8 days after therapy initiation. Imaging results were correlated with histopathology. In the results, IA chemotherapy showed a significant decrease in tumor volume (86.5 ± 15.6 %) compared to the IV chemotherapy (121.1 ± 39.6 %) and control (126.2 ± 22.0 %) 8 days after therapy ($p < 0.05$). Furthermore, IA chemotherapy resulted in a significant increase in mean tumor apparent diffusion coefficient (ADC) values (116.8 ± 44.9 %); in contrary IV chemotherapy (66.6 ± 26.9 %) and control (69.1 ± 29.5 %) showed a significant decrease in ADC values corresponding to further tumor growth ($p < 0.05$). However, there was no significant difference in perfusion parameters including initial area under the curve, K_{trans}, K_{ep}, and V_e between the groups ($p > 0.05$). Histopathology confirmed necrosis and necroptosis in the tumors after IA chemotherapy. In conclusion, IA chemotherapy may lead to effective inhibition of tumor cell proliferation and offer potential benefit of inducing higher degree of treatment response than IV chemotherapy.

Keywords Disease models · Injections · Intra-arterial · Brain neoplasms · Magnetic resonance imaging · Taxoids

Introduction

Brain metastasis is a major contributor to mortality and morbidity in patients with systemic cancer [1]. Radiation therapy, including whole-brain radiation therapy and stereotactic radiosurgery, is the most widely used method for treating brain metastasis, despite the fact that it provides poor outcomes with a median survival time of only 4–6 months [2, 3]. The role of systemic intravenous (IV) chemotherapy in the treatment of brain metastases has been limited, as the blood–brain barrier (BBB) prevents penetration of chemotherapeutic agents into brain tumors [4, 5]. In order to overcome the BBB, various approaches have been proposed. So-called intraarterial (IA) chemotherapy is an approach for increasing the effective concentration of a chemotherapy agent in central nervous system. This regional delivery technique can produce an increase in local plasma peak concentration and local area under the curve (AUC) related to the first pass effect, which translates to a significant 3–5.5-fold increase in intratumoral chemotherapy concentration [6, 7].

Electronic supplementary material The online version of this article (doi:10.1007/s11060-015-2041-5) contains supplementary material, which is available to authorized users.

✉ Keonha Kim
somatom@skku.edu

[1] Department of Radiology, Korea University Anam Hospital, Korea University College of Medicine, Seoul, Korea

[2] Department of Radiology, Samsung Medical Center, Sungkyunkwan University School of Medicine, 50, Irwon-dong, Gangnam-gu, Seoul 135-710, Korea

Magnetic resonance imaging (MRI) plays a major role in the current management of brain tumors, including diagnosis and response assessment following treatment [8]. Several tumor parameters extracted from diffusion-weighted imaging (DWI) and dynamic contrast-enhanced (DCE)-MRI have received attention as useful noninvasive biomarkers that can reflect cellular and vascular tumor responses to local or systemic treatment. Tumor apparent diffusion coefficient (ADC) changes in response to cytotoxic therapy reflect alterations in tumor cellularity that can be detected prior to distinct changes in tumor volume [9, 10]. DCE-MRI characterizes tumor perfusion and permeability as potential surrogate biomarkers for angiogenesis and has been utilized for measurement of tumor vascular response. The AUC directly calculated from the signal intensity versus time curve and the vascular transfer constant (K_{trans}) correlated well with tumor vascularity change in models of preclinical subcutaneous solid tumors, including glial tumors [11, 12]. Therefore, multiparametric MR analysis based on ADC- and DCE-derived parameters would provide comprehensive evaluation of tumor response to anticancer drugs.

Previously published series have investigated the therapeutic efficacy of IA chemotherapy for treatment of brain tumors in both animal and clinical studies [6, 13–17]. However, numerous limitations prevented precise evaluation of IA chemotherapy therapeutic efficacy under clinical conditions. Therefore, many investigators concurred that further preclinical trials are needed to establish the efficacy of IA chemotherapy [13, 15, 17]. In this study, we investigated treatment response to IA chemotherapy with DWI and DCE-MRI in an orthotopic xenograft mouse model of metastatic breast cancer. And furthermore we compared the therapeutic efficacy of IA chemotherapy with that of IV systemic chemotherapy in this model.

Materials and methods

Intracranial xenograft tumor model

All animal experiments were approved by the Institutional Animal Care and Use Committee. Thirty 8-week-old female BALB/c nude mice (20 ± 2.3 g) were used as a mouse xenograft model. Intracranial metastatic xenograft tumors were established by stereotactic-guided inoculation of 5×10^5 MDA-MB-231 breast cancer cells into the right caudate nucleus. The details of the orthotopic implant strategy are provided in online resource 1. During tumor cell implantation, therapy experiments, and MRI acquisition, animals were anesthetized by 1.0–1.5 % isoflurane inhalation in oxygen-enriched air via a nose cone. Tumor growth was monitored by MRI. When the largest diameter of the tumor reached 1.5 ± 0.5 mm, baseline MRI data including DWIs and DCE-MRI were acquired 1 day before therapy initiation (Day 0) (Fig. 1).

Therapy experiment

Docetaxel (Fluka®) was obtained from Sigma-Aldrich (St. Louis, MO, USA). In order to avoid systemic toxicity and obtain high local concentration of the drug, we incorporated docetaxel into a solvent that allowed IA injection. The solvent was formulated with 6 % ethanol and 94 % saline, and the mixture of docetaxel and solvent was diluted on the day of injection with sterile saline to a final concentration of 0.26 mg/ml.

Thirty tumor-bearing nude mice were randomized by weight into three groups at 3 or 4 weeks after tumor implantation. As treatment groups, the IA docetaxel (IA-D) group received single IA administration of 1 mg/kg docetaxel ($n = 10$), and the IV docetaxel (IV-D) group received single IV administration of 1 mg/kg docetaxel ($n = 10$). As a control, the IA solvent (IA-S) group was intraarterially injected with an equal volume of the solvent ($n = 10$). Follow-up MRI was undertaken 1 (Day 1) and 8 days (Day 8) after therapy initiation. Animals were weighed daily to monitor toxicity and the therapy experiments were terminated at Day 56.

For IA injection (1 mg/kg), a 2-cm longitudinal midline incision was made from the hyoid bone to the sternal notch. The right sternocleidomastoid and paratracheal muscles were retracted laterally and medially, respectively. The course of the right distal common carotid artery (CCA), carotid bifurcation, proximal external and internal carotid arteries (ICA) were exposed after removal of the lateral right one-third of the hyoid bone. The distal CCA was cannulated in an antegrade fashion using a polyethylene tube (Becton–Dickinson, MD, USA) with an outer diameter of 0.40 mm. The heat-shapeable tip of the tube was precisely manipulated to permit navigation, and the exact IA injection point was 3–5 mm within the ICA passing the ligated pterygopalatine artery. After a single injection of docetaxel solution or solvent only into the ICA, the cannula was removed, the CCA was ligated proximally, and the animal was allowed to recover. An IV injection (1 mg/kg) was given into the tail vein using a homemade 31-gauge butterfly needle.

Acquisition of MR imaging data

All MRI was obtained using a 7.0-T USR preclinical MR system (Bruker Biospin, Fällanden, Switzerland). A quadrature birdcage coil (inside diameter, 72 mm; Bruker Biospin) was used for excitation. Detailed information

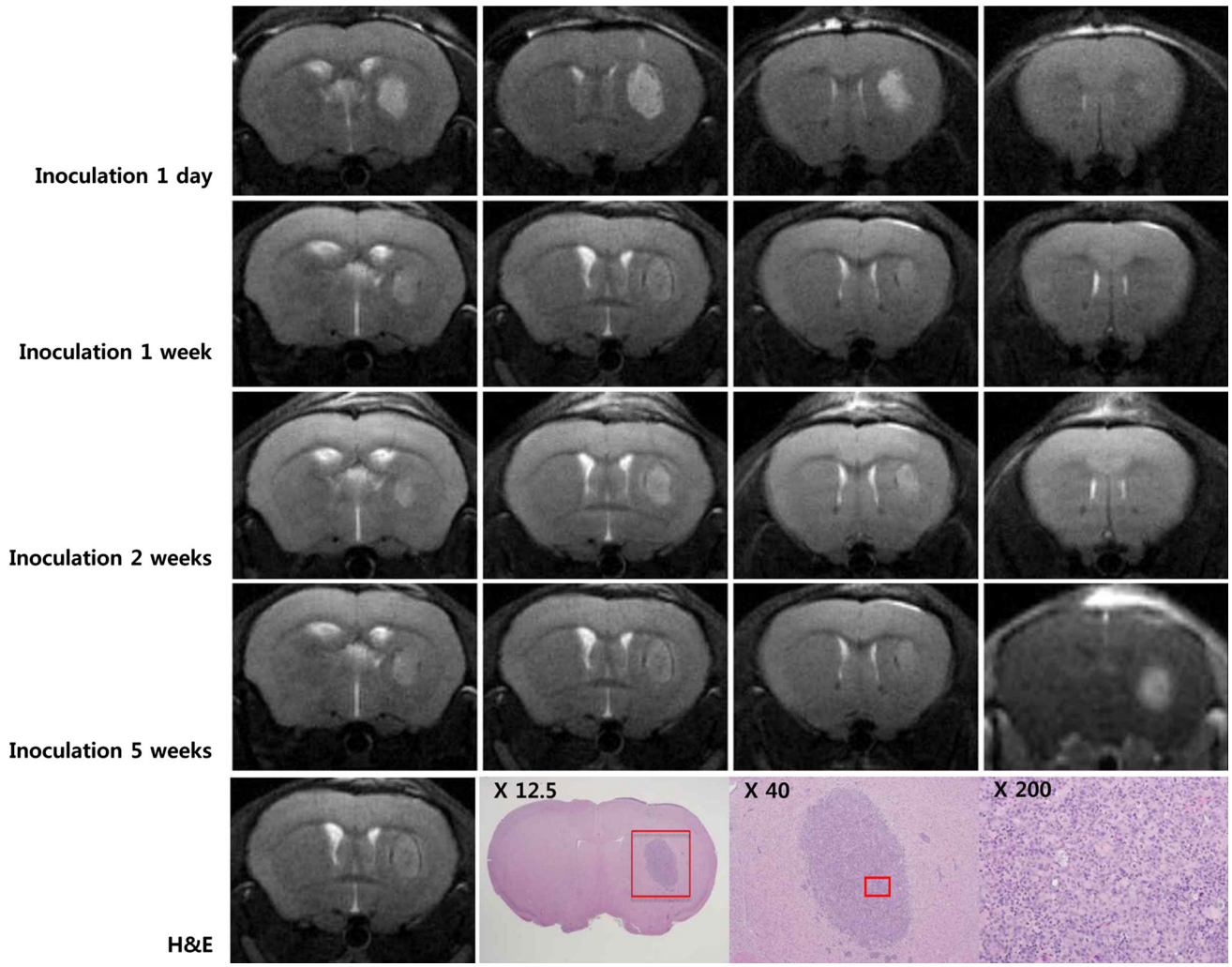

Fig. 1 Serial high-spatial-resolution coronal T2-weighted MR images of a mouse brain with time after stereotactic-guided inoculation of tumor cells. MR images for monitoring tumor growth were obtained 1 day, 1 week, 2 weeks, and 5 weeks following tumor cell inoculation. Note iso–hypo-intense lesion replacing the hyperintense tumor implant site 5 weeks after tumor inoculation. When the largest diameter of the tumor reached 1.5 ± 0.5 mm, baseline diffusion-weighted imaging and dynamic contrast-enhanced imaging (*first right image* 5 weeks after tumor inoculation) were obtained. Histopathology was performed on coronal sections obtained through the same rostro-caudal levels identified on T2-weighted MRI in our preliminary study. Hematoxylin–eosin-stained sections of intracranial MDA-MB-231 tumors from an untreated mouse showed successful tumor cell implantation and tumor growth

regarding MRI protocols with specific parameters and image processing are provided in online resource 2.

High-spatial-resolution coronal T2-weighted images (T2WIs) and corresponding DWIs were obtained. Image processing and manual segmentation of regions of interest (ROIs) were executed using a software package (Nordic ICE, NordicNeuroLab, Bergen, Norway). Tumor ROIs were manually delineated on T2WIs of 12 slices to measure tumor volumes, and these ROIs were transposed to the corresponding ADC maps. For diffusion analysis, the tumor ROIs were copied to similar normal contralateral regions of the brain. Even with respiratory gating, through-plane motion due to respiration resulted in slice-to-slice variation in ADC; therefore, tumor ADC was normalized to the contralateral brain ADC on each slice to account for this variation.

Coronal dynamic images were acquired with a T1-weighted fast low-angle shot sequence. Tumor ROIs on T2WIs of four sliced were manually defined, and transposed to the corresponding DCE maps. For perfusion analysis, the percent increase in contrast enhancement of the tumor ROIs on T1-weighted contrast enhancement images was normalized to the adjacent nontumoral region. The signal intensity course after IV injection of 100 μmol/kg gadoterate meglumine was monitored in the tumor for 7 min, and the area under the gadolinium concentration curve was calculated by numerical approximation. The initial AUC (*i*AUC) was calculated as the integrated contrast concentration over time

from contrast arrival at 0–60 s later. The contrast arrival time was determined by fitting an exponential curve to the upslope of the contrast concentration over time. A population-derived arterial input function (AIF) was utilized for general kinetic modeling and quantitative analysis of DCE-MRI to eliminate the need to calculate a subject-specific AIF.

Histopathology

At Day 8, three mice, one mouse per each group, were imaged and then euthanized to assess histologic treatment response associated with observed changes in MRI. Brains were fixed in 10 % paraformaldehyde for 48 h, and then fixed tissues were embedded in paraffin. Formalin-fixed paraffin-embedded specimens were serially sectioned into 5-μm thick sections for hematoxylin and eosin (H&E) stain. Histopathology was performed on coronal sections obtained through the same cranio-caudal levels that were previously identified by MRI as exhibiting tumor growth and treatment response.

Statistics

Statistical analyses were performed using SPSS version 20.0 software (SPSS, Chicago, IL, USA). Log-rank tests were used to compare survival rates among groups. The Kruskal–Wallis test was used to identify significant differences in parameters of DWI and DCE-MRI according to the mode of chemotherapy. Nonparametric analysis was adopted due to the small sample size of our experimental cohort, and statistical significance was defined as $p < 0.05$. When the results were considered to be significant on Kruskal–Wallis test, we performed a subsequent Mann–Whitney test to identify which of the treatment modality groups were different. Statistical significance was defined as $p < 0.016$ in the Mann–Whitney test due to Bonferroni's correction by three groups ($p < 0.05/3$ [number of comparisons]).

Results

Survival rate and tumor volume

All animals survived during the first 8 days after therapy initiation. A total of 27 mice were followed for survival since three mice were euthanized for histopathologic examination. The mean survival period was longer in the treatment groups compared to the controls, with the longest mean survival in the IA-D group (26.63 ± 9.02 days), followed by the IV-D group (25.38 ± 14.05 days), and then the IA-S group (23.14 ± 15.20 days). According to log-rank test, there was no significant difference in survival among groups ($p = 0.402$; Fig. 2).

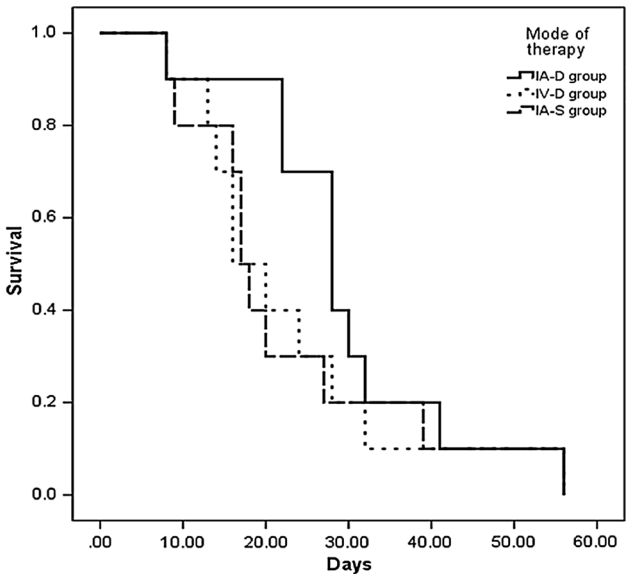

Fig. 2 The Kaplan–Meier survival plot of intraarterial docetaxel administration (IA-D, *solid line*), intravenous docetaxel administration (IV-D, *short-dashed line*), and intraarterial solvent injection (IA-S, *long-dashed line*) groups with a mean survival period of 26.63 ± 9.02 days (IA-D group), 25.38 ± 14.05 days (IV-D group), and 23.14 ± 15.20 days (IA-S group). There was no significant difference in survival rate among the groups on log-rank testing ($p = 0.402$)

The baseline mean tumor volumes of all three groups were similar (2.80–3.42 mm^3), although tumor volumes ranged from 1.06 to 7.12 mm^3 and varied slightly in location within the brain. The tumor growth rate was calculated according to percentage change in tumor volume from Days 0 to 8. Direct comparison of tumor growth rates of mice in each group was done, and the mean tumor percentage changes of each group was recorded (Table 1). Most notably, IA-D administration was successful, and there was a distinct reduction in the mean tumor volume in the IA-D group at Day 8 (86.5 ± 15.6 %). However, the mean tumor volumes of IV-D and IA-S groups continued to increase 8 days after therapy initiation. Statistical analyses demonstrated a significant attenuation of the tumor growth rate with IA-D administration compared to either IV-D or IA-S administration ($p < 0.05$). In addition, a significant difference in tumor growth rate was observed between the IA-D and IV-D groups ($p = 0.014$) and the IA-D and IA-S groups ($p = 0.001$) (refer to online resource 3).

MRI biomarkers

At baseline, we found that the normalized tumor ADC values were similar in all three groups, ranging from 51.2 to 53.8. The ADC response was quantified as the

Table 1 The percentage changes of tumor volumes, tumor ADC values, and perfusion parameters according to the mode of chemotherapy

	IA-D group Mean ± SD[c]	IV-D group Mean ± SD[c]	IA-S group Mean ± SD[c]	*p* value[a]
Tumor volume[b]				
Day 0	2.8 ± 1.4	3.4 ± 1.5	2.9 ± 1.0	
Day 8	2.2 ± 1.1	4.1 ± 1.8	3.5 ± 0.8	
Changes (%)	86.5 ± 15.6	121.1 ± 39.6	126.2 ± 22.0	0.005
nADC[b]				
Day 0	53.8 ± 20.1	51.6 ± 17.8		
Day 8	59.8 ± 21.4	34.9 ± 16.3	33.5 ± 20.8	
Changes (%)	116.8 ± 44.9	66.6 ± 26.9	69.1 ± 29.5	0.024
K^b_{trans}				
Day 0	0.043 ± 0.016	0.061 ± 0.021	0.049 ± 0.018	
Day 8	0.027 ± 0.014	0.056 ± 0.020	0.035 ± 0.019	
Changes (%)	79.9 ± 42.3	90.0 ± 47.7	72.6 ± 30.5	0.862
K^b_{ep}				
Day 0	0.07 ± 0.02	0.04 ± 0.02	0.04 ± 0.02	
Day 8	0.03 ± 0.02	0.03 ± 0.02	0.02 ± 0.01	
Changes (%)	53.6 ± 35.4	78.8 ± 50.6	70.5 ± 41.1	0.217
V_e				
Day 0	62.5 ± 31.4	93.8 ± 41.4	76.7 ± 26.7	
Day 8	37.1 ± 28.7	63.8 ± 36.8	57.6 ± 25.4	
Changes (%)	57.7 ± 51.6	67.1 ± 25.7	71.8 ± 32.6	0.681
*i*AUC				
Day 0	4.01 ± 1.78	6.57 ± 1.46	5.4 ± 2.01	
Day 8	2.56 ± 1.44	5.19 ± 1.24	3.92 ± 1.88	
Changes (%)	71.9 ± 27.7	73.1 ± 25.5	74.7 ± 61.3	0.598

[a] *p* values of the Kruskal–Wallis test

[b] Tumor volume (mm^3), nADC (normalized tumor apparent diffusion coefficient, unitless), K_{trans} (s^{-1}), K_{ep} (s^{-1})

[c] *SD* standard deviation

percentage change from the normalized tumor ADC at Days 0–8. The ADC response was significantly different according to both mode of chemotherapy administration and solvent injection ($p < 0.05$; Table 1). Specifically, treatment with IA-D administration resulted in a significant increase in the mean tumor ADC values compared to IV-D administration ($p = 0.001$) or IA-S injection ($p = 0.015$; online resource 2). There was no significant difference in ADC response between the IA-S and IV-D groups ($p > 0.016$). Corresponding histopathologic examination demonstrated a marked shrinkage of tumor cells after IA-D administration in mice with increased tumor ADC (Fig. 3) and a dense cellularity of tumor cells after IA-S injection in mice with decreased tumor ADC (Fig. 4).

For assessment of tumor perfusion response, the percentage change between tumor *i*AUC at Days 0 and 8 was calculated. The baseline whole tumor measurements of the *i*AUC values showed no significant differences among groups. Generally, all tumors exhibited a well-perfused rim and a central region with slightly lower values, and this characteristic was relatively maintained on Day 8 with a global decrease in *i*AUC values. Either IA or IV administration chemotherapy with docetaxel resulted in a decrease in *i*AUC at Day 8, however, there was no significant difference in changes in *i*AUC values among groups ($p > 0.05$). Furthermore, modified Tofts kinetic modeling using individual T1 and population-based AIF data demonstrated that there was no significant difference in DCE parameters including K_{trans}, K_{ep}, and V_e values among groups ($p > 0.05$).

Discussion

In the pre-clinical study, creation of a reliable tumor model was essential for assessment of the therapeutic efficacy of a new antitumor drug [18]. In brain tumor studies, therapies that have been effective in animal studies frequently show dismal performance in clinical trials. Many investigators have indicated that heterotopic models in which tumor cells

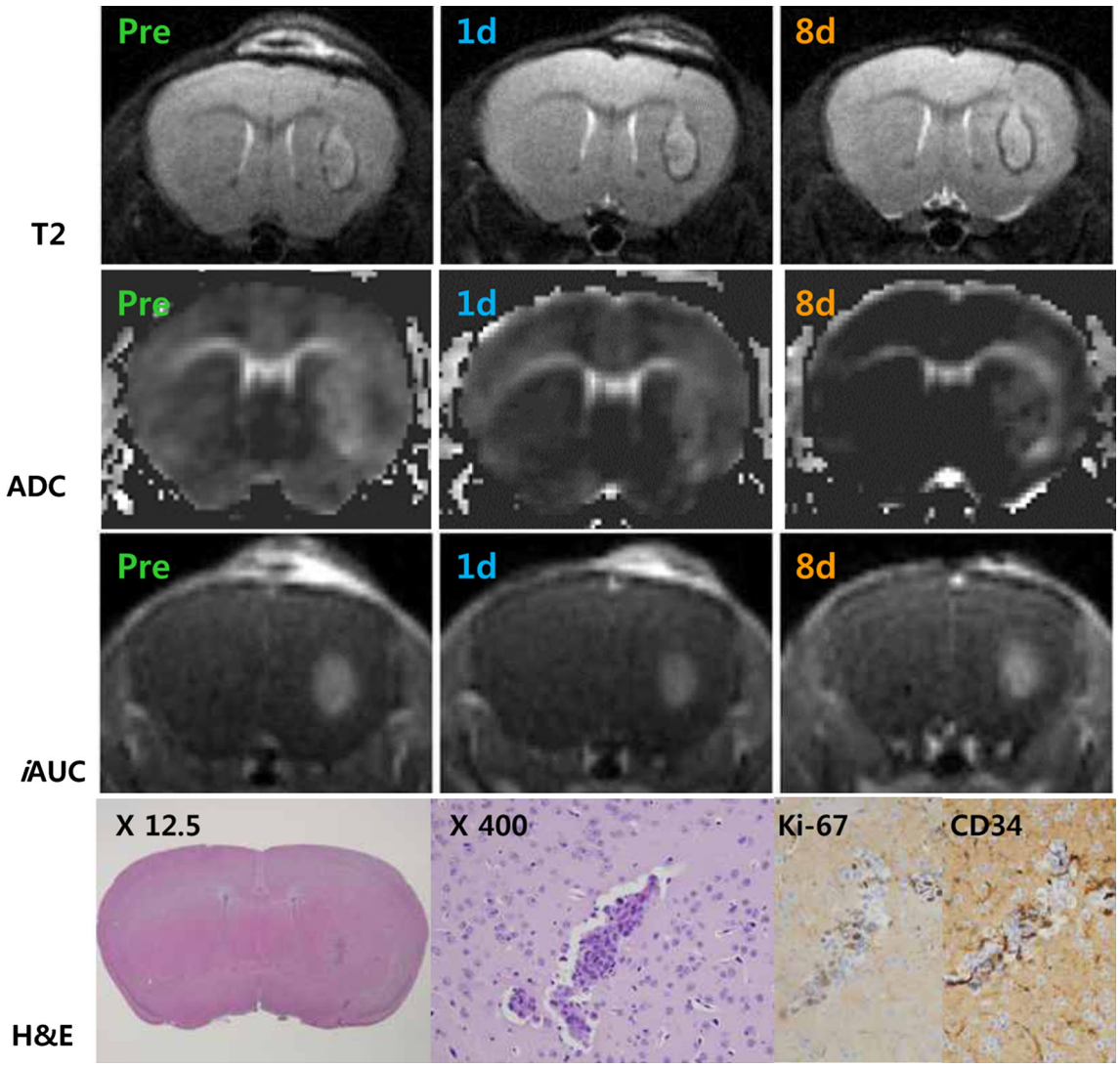

Fig. 3 Illustration of a MDA-MB-231 intracranial xenograft treated with a single intraarterial injection of docetaxel chemotherapy. Pretreatment T2-weighted MR image (T2WI) shows an irregularly shaped isointense lesion within hyperintense tumor inoculation site, indicating successful tumor growth. Serial T2WIs show mild shrinkage of the isointense lesion within the hyperintense tumor implantation site, and the mean tumor volume decreased from 1.36 to 1.18 mm^3. The corresponding ADC maps show an interval increase in the normalized tumor ADC values after treatment from 31.2 to 55.1. Hematoxylin–eosin-stained slides showed a marked shrinkage of tumor cells with an apparent coagulative necrosis. Mitotic count was up to 1 or 2 at ×400 magnification view and scanty vascularization was observed on immunohistochemistry of CD34. The dynamic contrast-enhanced images at 60 s exhibited a global decrease in tumor perfusion and permeability. The percentage change was 53.8 % in *i*AUC and 89.4 % in K_{trans}

were injected subcutaneously was one of the main reasons for this discrepancy [19]. Specifically, the tumor microenvironment is a significant factor in tumor growth and response to treatment [20]. An intracranial orthotopic model of brain tumors in animals has been developed, and stereotactic-guided inoculation of tumor cells allows precise implantation of brain tumors in small animal models. Although an orthotopic mouse brain tumor model might show spontaneous phenotype changes and altered physiologic processes derived from complex angiogenesis, several investigators have demonstrated qualitative and quantitative similarities between original tumors in humans and implanted tumor models in mice [21, 22]. In this study, we evaluated the therapeutic efficacy of IA administration chemotherapy in a MDA-MB-231 human breast cancer xenograft model in mice and assessed treatment response to IA chemotherapy using of MRI including DWI and DCE-MRI. Furthermore, IA chemotherapy with docetaxel showed a significant tumor regression with changes in ADC values as early as 8 days after treatment compared with IV systemic chemotherapy.

Tumor ADC is a sensitive imaging biomarker for the detection of early drug-induced cellular changes that precede macroscopic volumetric responses within a tumor

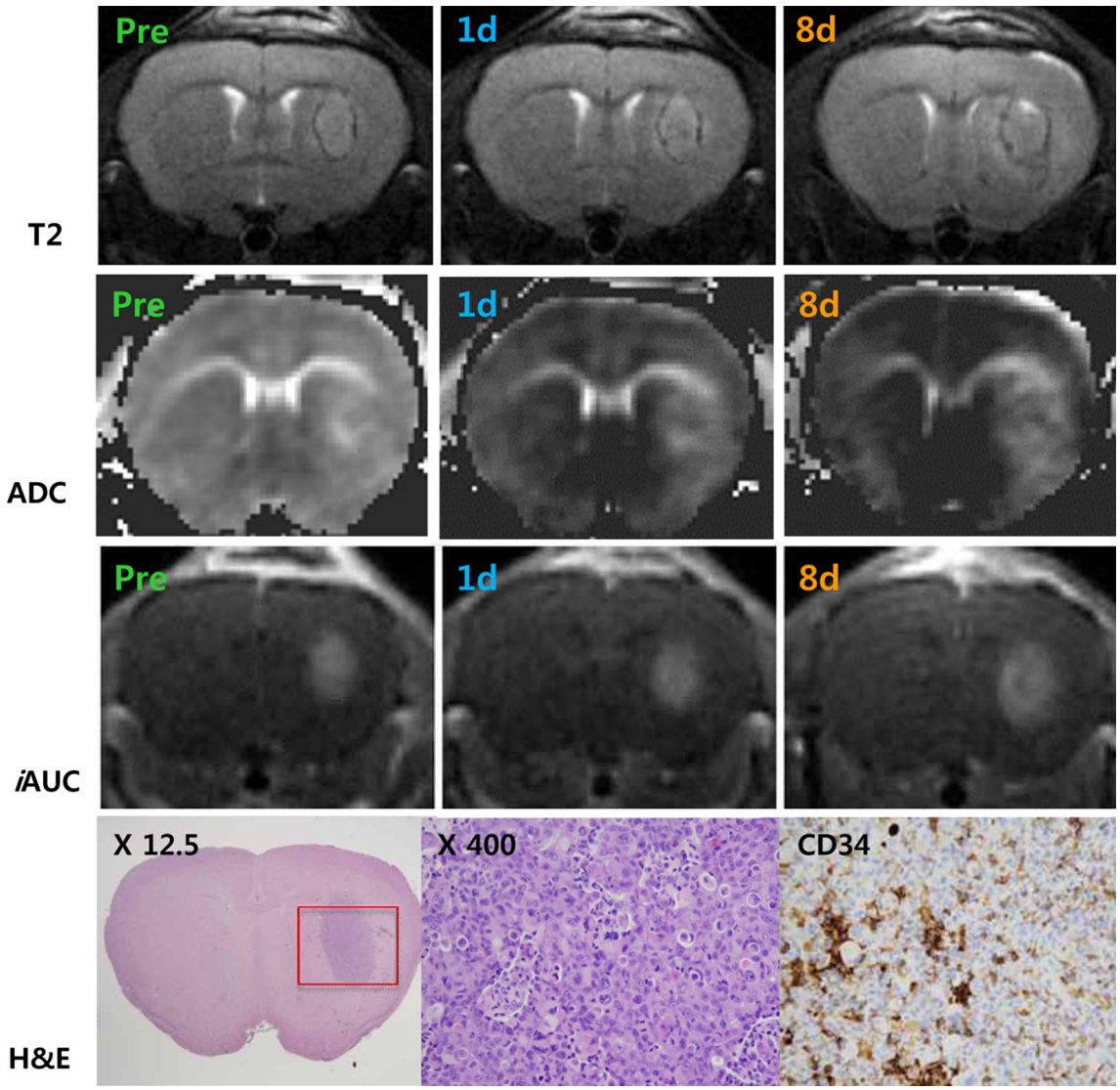

Fig. 4 Illustration of a MDA-MB-231 intracranial xenograft treated with a single intraarterial injection of solvent only. The isointense lesion replacing the entire hyperintense tumor inoculation site is delineated on pretreatment T2-weighted MR images. Eight days after therapy initiation, T2-weighted and dynamic contrast-enhanced images at 60 s show an interval increase in tumor size with contrast enhancement. The percentage changes of tumor volume and mean tumor ADC values were 131.4 % (1.96–2.58 mm^3) and 46.9 % (50.0–23.4), respectively. Representative hematoxylin–eosin-stained section obtained 8 days after therapy showed compact cellularity with scanty coagulative necrosis. Mitotic count was up to 5 at ×400 magnification view and deformed vascular structure with peripheral location was revealed on immunohistochemistry of CD34. Marked reduction in the mean tumor ADC values correlated well with these histological findings

[23, 24]. It can provide early prediction of treatment response without the long delay involved in reaching a clinical endpoint [9]. In our results, IA administered chemotherapy resulted in an increase of ADC values 8 days after onset of therapy paralleled by regression of overall tumor volume, whereas IV systemic chemotherapy and the control group showed a significant decrease in ADC values 8 days after therapy initiation corresponding to further tumor growth. The difference in chemotherapy efficacy appears dependent on the mode of docetaxel administration, which can be explained in terms of the efficiency in crossing the BBB with IA administration. However, interpretation of ADC response to anticancer agents is difficult and complex due to the heterogeneity of human brain tumors and complex interactions between microcellular and microperfusion changes [9, 25, 26]. Given similar pretreatment tumor ADC values and similar changes in posttreatment perfusion parameters among groups, we speculated that the effect of tumor heterogeneity and microperfusion changes might be mitigated in the present study. Histopathology demonstrated necrosis and apoptosis in the tissue samples in the IA chemotherapy

group. Thus, less viable tumor cells in histopathology are well correlated with less restricted tissue water movement on imaging. Nevertheless, further studies utilizing functional diffusion maps are needed to develop clinical applicability of ADC values as an imaging biomarker [9, 26].

DCE-MRI provides information on the microvascular environment of tumors, and is used to provide imaging biomarkers reflecting the degree of neoangiogenesis and altered functional properties of microvasculature following treatment [27]. The *i*AUC is a parameter that resembles the perfusion and permeability characteristics as well as the interstitial volume of the tumor [28, 29]. International consensus panels recommended 60 s as the exact cutoff time for calculation of *i*AUC with a reasonable strength of correlation with K_{trans} [29]. In this study, we compared the effect of IA administration of docetaxel with the effect of IV administration of docetaxel on tumor gadoterate meglumine exposure, by calculation of *i*AUC, K_{trans}, K_{ep}, and V_e values. To exclude direct toxic effect of solvent on tumor vasculature, we intraarterially injected solvent only for mice in the IA-S group as a control. However, there was no significant difference in the perfusion parameters including *i*AUC, K_{trans}, K_{ep}, and V_e values among groups. Several factors including vascular toxicity of the injected solvent and procedure-related ischemic complications may contribute to the reduction of perfusion parameters in the control group. The results show that docetaxel, a cytotoxic compound with antimitotic activity, has no measurable early impact on perfusion and permeability of orthotopic mouse brain tumor models. In addition, the individual tumor volume response to either mode of chemotherapy showed no association with subsequent response of perfusion parameters.

There were several limitations to our study. Our in vivo investigations were based on a limited number of animals with the same orthotopic cancers and similar grades and sizes. Further studies are needed concerning inter- and intraindividual variability of multiparametric imaging from a larger number of animals. In addition, the difficulty of acquiring DWIs and DCE-MRI with appropriate spatial and temporal resolution is another limitation of the present study. Based on the present protocol for acquiring DCE data, it is impossible to obtain subject-specific AIF values due to limited spatial resolution. This is one of the factors that motivated us to adopt a population-based AIF, and therefore substantial variation between subjects is a potential limitation. Instead, we included the *i*AUC value, which is easy to calculate, reproducible, and routinely used as a biomarker in drug trials [30]. The heterogeneity of tumor components also made it difficult to define reproducible ROIs. Some stereotaxically implanted tumor models had viable tumor components along the needle tract, even in the skull and scalp. The authors excluded extraaxial components of the tumor from analysis in order to exclude the effects of extraaxial blood supply to the tumor. Finally, the toxicity-induced weight profile is insufficient for assessing neurotoxicity in the brain and eye. Complete autopsy of all animals at death is needed to further investigate neurotoxicity relevant to IA chemotherapy in future experiments.

In conclusion, this study found that IA chemotherapy may substantially enhance tu

mor growth attenuation with tumor cell necrosis over IV systemic chemotherapy in a preclinical metastatic brain tumor model. In addition, treatment monitoring of IA chemotherapy using DWI and DCE-MRI was feasible. Specifically, DWI is a promising imaging modality for treatment monitoring; it shows a high percentage change in ADC value after treatment and a fair correlation with standard tumor volume change. However, the response assessment with DCE-MRI was less sensitive and conclusive in the study with cytotoxic chemotherapeutic agents. Further clinical trials are needed to validate the feasibility and clinical efficacy of IA chemotherapy.

Conflict of Interest The authors have no conflicts of interest to declare.

Ethical approval The authors followed all applicable international, national, and/or institutional guidelines for the care and use of animals in the present study.

References

1. Soffietti R, Ruda R, Trevisan E (2008) Brain metastases: current management and new developments. Curr Opin Oncol 20(6): 676–684. doi:10.1097/CCO.0b013e32831186fe
2. Kocher M, Soffietti R, Abacioglu U, Villa S, Fauchon F, Baumert BG, Fariselli L, Tzuk-Shina T, Kortmann RD, Carrie C, Ben Hassel M, Kouri M, Valeinis E, van den Berge D, Collette S, Collette L, Mueller RP (2011) Adjuvant whole-brain radiotherapy versus observation after radiosurgery or surgical resection of one to three cerebral metastases: results of the EORTC 22952-26001 study. J Clin Oncol Off J Am Soc Clin Oncol 29(2):134–141. doi:10.1200/JCO.2010.30.1655
3. Nieder C, Grosu AL, Gaspar LE (2014) Stereotactic radiosurgery (SRS) for brain metastases: a systematic review. Radiat Oncol 9:155. doi:10.1186/1748-717X-9-155
4. Sanson M, Napolitano M, Yaya R, Keime-Guibert F, Broet P, Hoang-Xuan K, Delattre JY (2000) Second line chemotherapy with docetaxel in patients with recurrent malignant glioma: a phase II study. J Neurooncol 50(3):245–249
5. Pardridge WM (2005) The blood–brain barrier: bottleneck in brain drug development. NeuroRx J Am Soc Exp Neurother 2(1):3–14. doi:10.1602/neurorx.2.1.3
6. Newton HB, Slivka MA, Volpi C, Bourekas EC, Christoforidis GA, Baujan MA, Slone W, Chakeres DW (2003) Intra-arterial carboplatin and intravenous etoposide for the treatment of metastatic brain tumors. J Neurooncol 61(1):35–44

7. Newton HB, Figg GM, Slone HW, Bourekas E (2006) Incidence of infusion plan alterations after angiography in patients undergoing intra-arterial chemotherapy for brain tumors. J Neurooncol 78(2):157–160. doi:10.1007/s11060-005-9080-2
8. Chung C, Jalali S, Foltz W, Burrell K, Wildgoose P, Lindsay P, Graves C, Camphausen K, Milosevic M, Jaffray D, Zadeh G, Menard C (2013) Imaging biomarker dynamics in an intracranial murine glioma study of radiation and antiangiogenic therapy. Int J Radiat Oncol Biol Phys 85(3):805–812. doi:10.1016/j.ijrobp.2012.07.005
9. Moffat BA, Chenevert TL, Meyer CR, McKeever PE, Hall DE, Hoff BA, Johnson TD, Rehemtulla A, Ross BD (2006) The functional diffusion map: an imaging biomarker for the early prediction of cancer treatment outcome. Neoplasia 8(4):259–267. doi:10.1593/neo.05844
10. Chenevert TL, McKeever PE, Ross BD (1997) Monitoring early response of experimental brain tumors to therapy using diffusion magnetic resonance imaging. Clin Cancer Res Off J Am Assoc Cancer Res 3(9):1457–1466
11. Hillman GG, Singh-Gupta V, Zhang H, Al-Bashir AK, Katkuri Y, Li M, Yunker CK, Patel AD, Abrams J, Haacke EM (2009) Dynamic contrast-enhanced magnetic resonance imaging of vascular changes induced by sunitinib in papillary renal cell carcinoma xenograft tumors. Neoplasia 11(9):910–920
12. Bradley DP, Tessier JJ, Lacey T, Scott M, Jurgensmeier JM, Odedra R, Mills J, Kilburn L, Wedge SR (2009) Examining the acute effects of cediranib (RECENTIN, AZD2171) treatment in tumor models: a dynamic contrast-enhanced MRI study using gadopentate. Magn Reson Imaging 27(3):377–384. doi:10.1016/j.mri.2008.07.021
13. Fortin D, Gendron C, Boudrias M, Garant MP (2007) Enhanced chemotherapy delivery by intraarterial infusion and blood–brain barrier disruption in the treatment of cerebral metastasis. Cancer 109(4):751–760. doi:10.1002/cncr.22450
14. Fortin D, Desjardins A, Benko A, Niyonsega T, Boudrias M (2005) Enhanced chemotherapy delivery by intraarterial infusion and blood–brain barrier disruption in malignant brain tumors: the Sherbrooke experience. Cancer 103(12):2606–2615. doi:10.1002/cncr.21112
15. Boyle FM, Eller SL, Grossman SA (2004) Penetration of intra-arterially administered vincristine in experimental brain tumor. Neurooncology 6(4):300–305. doi:10.1215/S1152851703000516
16. Gobin YP, Cloughesy TF, Chow KL, Duckwiler GR, Sayre JW, Milanese K, Vinuela F (2001) Intraarterial chemotherapy for brain tumors by using a spatial dose fractionation algorithm and pulsatile delivery. Radiology 218(3):724–732. doi:10.1148/radiology.218.3.r01mr41724
17. Doolittle ND, Miner ME, Hall WA, Siegal T, Jerome E, Osztie E, McAllister LD, Bubalo JS, Kraemer DF, Fortin D, Nixon R, Muldoon LL, Neuwelt EA (2000) Safety and efficacy of a multicenter study using intraarterial chemotherapy in conjunction with osmotic opening of the blood–brain barrier for the treatment of patients with malignant brain tumors. Cancer 88(3):637–647
18. Fei XF, Zhang QB, Dong J, Diao Y, Wang ZM, Li RJ, Wu ZC, Wang AD, Lan Q, Zhang SM, Huang Q (2010) Development of clinically relevant orthotopic xenograft mouse model of metastatic lung cancer and glioblastoma through surgical tumor tissues injection with trocar. J Exp Clin Cancer Res 29:84. doi:10.1186/1756-9966-29-84
19. Rosol M, Harutyunyan I, Xu J, Melendez E, Smbatyan G, Finlay JL, Krieger MD, Gonzalez-Gomez I, Reynolds CP, Nelson MD, Erdreich-Epstein A, Bluml S (2009) Metabolism of orthotopic mouse brain tumor models. Mol Imaging 8(4):199–208
20. Hanahan D, Weinberg RA (2000) The hallmarks of cancer. Cell 100(1):57–70
21. Simoes RV, Garcia-Martin ML, Cerdan S, Arus C (2008) Perturbation of mouse glioma MRS pattern by induced acute hyperglycemia. NMR Biomed 21(3):251–264. doi:10.1002/nbm.1188
22. van der Sanden BP, Rijken PF, Heerschap A, Bernsen HJ, van der Kogel AJ (1997) In vivo (31)P magnetic resonance spectroscopy and morphometric analysis of the perfused vascular architecture of human glioma xenografts in nude mice. Br J Cancer 75(10):1432–1438
23. Roth Y, Tichler T, Kostenich G, Ruiz-Cabello J, Maier SE, Cohen JS, Orenstein A, Mardor Y (2004) High-b-value diffusion-weighted MR imaging for pretreatment prediction and early monitoring of tumor response to therapy in mice. Radiology 232(3):685–692. doi:10.1148/radiol.2322030778
24. Chenevert TL, Stegman LD, Taylor JM, Robertson PL, Greenberg HS, Rehemtulla A, Ross BD (2000) Diffusion magnetic resonance imaging: an early surrogate marker of therapeutic efficacy in brain tumors. J Natl Cancer Inst 92(24):2029–2036
25. Dassler K, Scholle FD, Schutz G (2014) Dynamic gadobutrol-enhanced MRI predicts early response to antivascular but not to antiproliferation therapy in a mouse xenograft model. Magn Reson Med Off J Soc Magn Reson Med/Soc Magn Reson Med 71(5):1826–1833. doi:10.1002/mrm.24815
26. Moffat BA, Chenevert TL, Lawrence TS, Meyer CR, Johnson TD, Dong Q, Tsien C, Mukherji S, Quint DJ, Gebarski SS, Robertson PL, Junck LR, Rehemtulla A, Ross BD (2005) Functional diffusion map: a noninvasive MRI biomarker for early stratification of clinical brain tumor response. Proc Natl Acad Sci USA 102(15):5524–5529. doi:10.1073/pnas.0501532102
27. Kiessling F, Farhan N, Lichy MP, Vosseler S, Heilmann M, Krix M, Bohlen P, Miller DW, Mueller MM, Semmler W, Fusenig NE, Delorme S (2004) Dynamic contrast-enhanced magnetic resonance imaging rapidly indicates vessel regression in human squamous cell carcinomas grown in nude mice caused by VEGF receptor 2 blockade with DC101. Neoplasia 6(3):213–223. doi:10.1593/neo.3394
28. Li SP, Padhani AR (2012) Tumor response assessments with diffusion and perfusion MRI. J Magn Reson Imaging 35(4):745–763. doi:10.1002/jmri.22838
29. Leach MO, Brindle KM, Evelhoch JL, Griffiths JR, Horsman MR, Jackson A, Jayson GC, Judson IR, Knopp MV, Maxwell RJ, McIntyre D, Padhani AR, Price P, Rathbone R, Rustin GJ, Tofts PS, Tozer GM, Vennart W, Waterton JC, Williams SR, Workman P, Pharmacodynamic/Pharmacokinetic Technologies Advisory Committee DDOCRUK (2005) The assessment of antiangiogenic and antivascular therapies in early-stage clinical trials using magnetic resonance imaging: issues and recommendations. Br J Cancer 92(9):1599–1610. doi:10.1038/sj.bjc.6602550
30. Jesberger JA, Rafie N, Duerk JL, Sunshine JL, Mendez M, Remick SC, Lewin JS (2006) Model-free parameters from dynamic contrast-enhanced-MRI: sensitivity to EES volume fraction and bolus timing. J Magn Reson Imaging 24(3):586–594. doi:10.1002/jmri.20670